pH dependent hydration change in a Gd based MRI contrast agent with a phosphonated ligand

Cyrille Charpentier, Jérémy Salaam, Aline M. Nonat, Fabio Carniato, Olivier Jeannin, Isabel Brandariz, David Esteban-Gómez, Carlos Platas-Iglesias, Loic Joanny Charbonnière, Mauro Botta

pH dependent hydration change in a Gd based MRI contrast agent with a phosphonated ligand

Cyrille Charpentier,[a] Jérémy Salaam,[a] Aline Nonat,[a] Fabio Carniato,[b] Olivier Jeannin,[c] Isabel Brandariz,[d] David Esteban Gomez,[d] Carlos Platas-Iglesias,[d]* Loïc J. Charbonnière,[a]* and Mauro Botta[b]*

Dedicated to Pr Jean-Pierre Sauvage on the occasion of his 75Th birthday

Abstract: The heptadentate ligand L was shown to form extremely stable Gd complex at neutral pH with a pGd value of 18.4 at pH 7.4. The X-ray crystal structures of the complexes formed with Gd and Tb displayed two very different coordination behaviors being respectively octa- and nonacoordinated. The relaxometric properties of the Gd complex were studied by field dependent relaxivity measurements at various temperatures and by ^{17}O NMR spectroscopy. The pH dependence of the longitudinal relaxivity profile indicated large changes around neutral pH leading to a very large value of 10.1 $mM^{-1}\cdot s^{-1}$ (60 MHz, 298 K) at pH 4.7. The changes were attributed to an increase of the hydration number from one water molecule in basic conditions to two at acidic pH. A similar trend was observed for the luminescence of the Eu complex, confirming the change in hydration state. DOSY experiments were performed on the Lu analogue, pointing to the absence of dimers in solution in the considered pH range. A breathing mode of the complex was postulated, further supported by ^{1}H and ^{31}P-NMR spectroscopy of the Yb complex at varying pH and was finally modeled by DFT calculations.

Introduction

Magnetic Resonance Imaging (MRI) is a major technique in the diagnostic toolbox of clinicians and Gd based complexes have largely demonstrated their efficiency as contrast agents to accelerate the relaxation of neighboring protons and hence improve the quality of the images.[1] If current fundamental efforts seems to be directed towards new developments such as the use of paraCEST agents,[2] other paramagnetic cations such as Mn^{2+} or Ni^{2+},[3] or even other nuclei of interest such as ^{19}F,[4] there is still a need for a better basic understanding of the structure/relationship activity of Gd based contrast agents.

Interestingly, despite some very attractive properties, phosphonated ligands have been far less studied than their carboxylated analogues for the complexation of lanthanides in general and Gd in particular. This may be correlated with a more complex coordination behavior with multiple coordinating modes[5] and complex charge states, depending on the pH of the solution. But these bulkier functions generally engender increased stabilities of the formed complexes,[6] and large second sphere interactions that may positively affect the relaxation properties.[7] However, it was soon recognized that the coordination behavior of phosphonated ligands, and particularly 2-pyridine-phosphonic acid[8a-c] may be affected by the formation of polynuclear species in solution,[8d-f] and this could be advantageously used to engineer the formation of complex heteropolynuclear edifices.[9]

In an effort to design new polyphosphonated ligands for Ln coordination, we recently reported the synthesis of ligand L (Scheme 1),[10] a tripodal ligand based on three 6-phosphono-2-methylene-pyridyl arms grafted on a central N atom. L forms very stable [LnL] complexes with lanthanide cations in aqueous solutions, with additional polynuclear species in the presence of excess of cations. Considering the heptadenticity of L, one would logically expect its Gd complex to contain water molecules in its first coordination sphere with concomitant appealing relaxivity properties. We here present a thorough investigation of the relaxivity properties of [GdL] and show that it presents a very interesting change of its hydration number as a function of the pH of the solution.

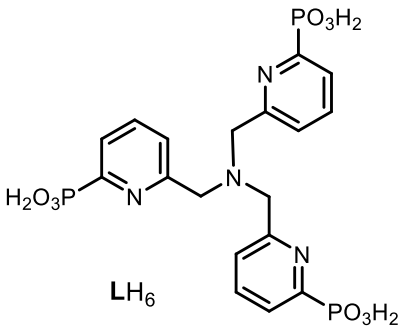

Scheme 1. Podand type phosphonated ligand LH_6

[a] C. Charpentier, J. Salaam, Dr A. Nonat, Dr L.J. Charbonnière
Equipe de Synthèse Pour l'Analyse (SynPA), Institut Pluridisciplinaire Hubert Curien, UMR 7178 CNRS/Université de Strasbourg, ECPM, 25 rue Becquerel, Bâtiment R1N0, 67087, Strasbourg Cedex 02, France.
[b] F. Carniato Pr M. Botta,
Dipartimento di Scienze e Innovazione Tecnologica, Università del Piemonte Orientale, Viale T. Michel 11, 15121 Alessandria, Italy.
E-mail : mauro.botta@uniupo.it
[c] Dr O. Jeannin
Université de Rennes, CNRS, ISCR-UMR6226, F-35000 Rennes, France.
[d] I. Brandariz, Dr D. Esteban-Gomez, Dr C. Platas-Iglesias,
Centro de Investigacións Científicas Avanzadas (CICA) and Departamento de Química, Universidade da Coruña, Campus da Zapateira-Rúa da Fraga 10, 15008 A Coruña, Spain.
E-mail : cplatas@udc.es

Supporting information for this article is given via a link at the end of the document

Results and Discussion

Protonation constants of L and stability constants of the Gd complex. The protonation constants of the L^{6-} ligand were determined using potentiometric titrations at 25 ºC and ionic strength adjusted to 0.15 M NaCl. The results are compared in Table 1 with the protonation constants reported for the related tripodal ligands $TPAA^{3-}$ and NTA^{3-}, respectively functionalized by 2-methylenepyridine-6-carboxilic acid and acetic acid functions. The first protonation constant of L^{6-} ($\log K_1 = 8.58$) is intermediate with respect to those reported for $TPAA^{3-}$ and NTA^{3-}. Thus, we assigned this protonation step to the protonation of the amine nitrogen atom of the ligand. The substitution of the acetate groups of NTA^{3-} by picolinate groups is known to provoke a decrease of the basicity of the neighboring amine nitrogen atoms in polyaminopolycarboxylate ligands,[11] but this effect is less pronounced in the case of pyridine-2-yl-phosphonate groups. The three subsequent protonation constants of L^{6-} are assigned to the protonation of the phosphonate groups of the ligand. The log*K* values are similar to the protonation constants commonly observed for phosphonated ligands. [12,13] The lowest protonation constant that could be determined with potentiometric titrations was $\log K_6$ which was also corroborated by spectrophotometric titrations (Table 1 and Figure S1, Supporting Information)).

Table 1. Ligand protonation constants and stability and protonation constants of the Gd^{3+} complex of L^{6-} (25 ºC, *I* = 0.15 M NaCl) and related ligands reported in the literature. [14,15]

	L^{6-} [a]	$TPAA^{3-}$ [c]	NTA^{3-} [d]
$\log K_1$	8.58(1)	6.78	9.65
$\log K_2$	7.66(1)	4.11	2.48
$\log K_3$	6.81(2)	3.3	1.84
$\log K_4$	5.03(3)	2.5	
$\log K_5$	2.91(6)		
$\log K_6$	2.16(6)		
	2.02(2) [b]		
$\log K_{GdL}$	18.97(2) [b]	10.2	11.54
$\log K_{GdHL}$	7.24(2)		
$\log K_{GdH_2L}$	4.22(2)		
$\log K_{GdH_3L}$	2.89(2) [b]		
pGd [e]	18.4	11.1	10.2

[a] The values within parentheses represent the standard deviations of the last significant digit. All values were obtained with potentiometric titrations, unless otherwise stated. [b] Values obtained with spectrophotometric titrations. [c] Data from reference 14 (25 ºC, *I* = 0.1 M KCl). [d] Data from reference 15 (25 ºC, *I* = 0.1 M KNO_3). [e] Defined as $-\log[Gd]_{free}$ at pH 7.4 for $[Gd]_{total}$ = 1 μM and $[L]_{total}$ = 10 μM.

The stability and protonation constants of the GdL^{3-} complex were initially investigated using potentiometric titrations in 0.15 M NaCl at 25 ºC. However, the complex was found to be almost quantitatively formed at the beginning of the potentiometric titration at pH ~ 2. Thus, we decided to use spectrophotometric titrations in the pH range 1.9-0.8 to determine the stability constant of the complex (Figure 1). The combined analysis of potentiometric and spectrophotometric titration data afforded a stability constant of logKGdL = 18.97(2) and the protonation constants of the complex (Table 1) This stability constant is eight orders of magnitude higher than that of the GdTPAA complex, which contains picolinate groups, and seven orders of magnitude higher than that of GdNTA.

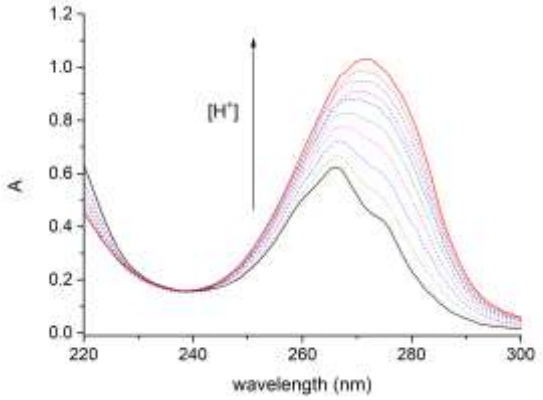

Figure 1. UV absorption spectra of an 1:1 Gd^{3+}:L mixture (4.8×10^{-5} M, 0.15 M NaCl, 25°C) recorded at different pH values from 1.9 (black line, 12.5% free Gd^{3+}) to 0.8 (red line, 96% of free Gd^{3+}).

The analysis of the data afforded three protonation constants (Table 1), each corresponding to the protonation of one of the phosphonate groups of the ligand. The species distribution diagram (Figure 2) shows that protonation of the complex occurs below pH ~ 10, with the $GdHL^{2-}$ form reaching an abundance of 94% at pH 5.7. The GdH_2L^{-} species is formed below pH ~ 7.0 (maximum abundance of 70% at pH 3.6). Below that pH, the neutral GdH_3L form of the complex predominates until pH ~1.

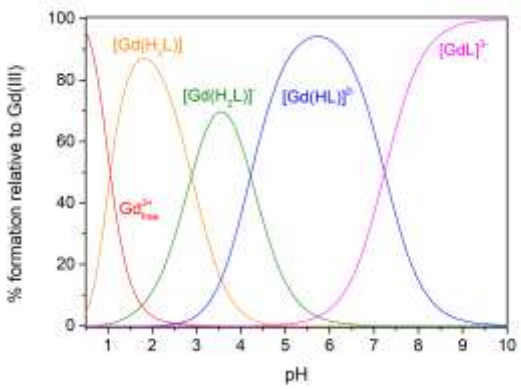

Figure 2. Species distribution diagram calculated for the Gd:L system with $[Gd^{3+}] = [L] = 10^{-3}$ M.

Complex dissociation occurs below pH ~ 3, with free Gd^{3+} representing only 2.7% of the overall Gd^{3+} concentration at pH 2.0. The conditional stability of the GdL complex at pH 7.4 was assessed by calculating a pGd value[16] of 18.4 for GdL,which is very high compared to those of the TPAA and NTA analogues, and slightly lower than those reported for tripodal Gd^{3+} complexes of the HOPO family (typically pGd = 20-21).[17] The pGd value of GdL compares well to those of commercially available contrast agents such as $GdDTPA^{2-}$ (19.1) and GdDTPA-BMA (15.8).[18]

Synthesis and characterization of the [LnL] complexes. The [LnL] complexes were obtained by mixing equimolar amounts of the ligand and the Ln salts in aqueous solutions followed by neutralisation.[10] In acidic aqueous solution containing formic acid, the ES/MS spectrum of the Gd complex (Figure S2) unambiguously confirms the presence of the GdL complex with peaks at 685.96 m/z and 707.95 units having the perfect expected isotopic distribution for $[Gd(L\text{-}3H)H]^+$ and $[Gd(L\text{-}3H)Na]^+$ (Figure S3). In addition, one can also notice the presence of peaks corresponding to monocharged dimeric species at 1370.91 (attributed to $[(Gd(L\text{-}3H))_2H]^+$) and 1391.90 m/z units (attributed to $[(Gd(L\text{-}3H))_2Na]^+$) as well as a doubly charged dimer at 696.96 ($[(Gd(L\text{-}3H))_2HNa]^{2+}$) and peaks corresponding to $[(Gd(L\text{-}3H))_2H_2]^{2+}$ and $[(Gd(L\text{-}3H))_2Na_2]^{2+}$ partly hidden by the massives of the corresponding monomers, but faintly evidenced by the appearance of peaks separated by 0.5 m/z units (Figure S4). Finally, broad peaks are observed centered at 1370.91, 1391.90 m/z units that were attributed to doubly charged trimers (resp. $[(Gd(L\text{-}3H))_3H_2]^{2+}$ and $[(Gd(L\text{-}3H))_3HNa]^{2+}$). However, the presence of these polymeric species has to be taken with great care and may not be representative of the composition of the solution due to the concentration effect leading to high local concentrations with highly acidic medium during the nebulization process of electrospray.[19]

Solid state structure of the complexes. Slow evaporation of aqueous solutions of the Tb and Gd complexes afforded single-crystals suitable for X-ray diffraction analysis. Table S1 summarizes the main crystallographic data and structure refinement parameters for the two complexes.

Figure 3 represents views of the solid state structure of the Gd complex. The chemical formula of the structure is $[(GdL(H_2O))Na_3]_3.48H_2O$, where L stands for the fully deprotonated ligand. One can notice the very large number of water molecules for which the H atoms could not be refined in the structure. The basic unit is composed of three kinds of [GdL] complexes denoted 1 to 3. Gd1 and Gd2 are forming clusters containing four GdL complexes linked together by a set of 12 Na atoms, the cluster containing an inversion center. The last GdL (Gd3) complex is isolated and linked to a set of three Na^+ cations. For all GdL type of complex, the Gd atoms are octacoordinated and the coordination sphere around Gd is composed of the central N atom of the ligand, three N from the pyridyl arms, three oxygen atoms from the phosphonate functions and one oxygen atom from a water molecule. For Gd2L, the link with the Na^+ cation occurs through a single oxygen atom of a phosphonate function bound to Gd2, while for Gd1 and Gd3, the neighboring Na^+ cation is coordinated by two O atoms of two phosphonate functions coordinated to the Gd atom. As already observed for other phosphonated-based Ln complexes such as the Eu [20a] or Gd [20b] complex of DOTP (DOTP = 1,4,7,10-tetraazacyclododecane-1,4,7,10-tetrakis(methylenephosphonic acid)), or for the Eu complex of ligand L,[10] the complexes are forming layers, in which the GdL complexes are sandwiched between layers of Na^+ cations (Figure S5 and S6). Such structures result in the presence of numerous water molecules for the solvation of the complexes on the one hand and the clusters formed by the counterions on the other hand.

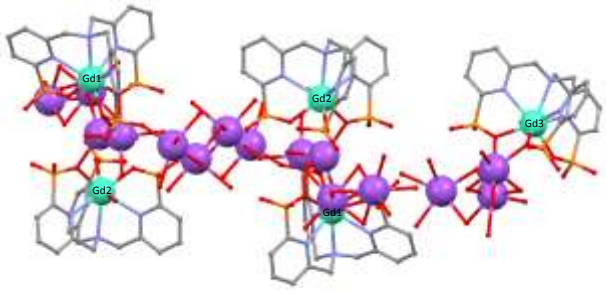

Figure 3. X-ray crystal structure of the [GdL] complex showing the three types of [GdL] complexes present in the cell (see text).

In contrast, the solid state structure of the Tb complex (Figure 4) is present in the form of dimers in which two TbL chelate units are linked through a complex set of stacking interactions, inter-complex bonds and bridging Na^+ cations. The chemical fomula of the structure is $[(TbLH_2(H_2O))Na]_2.4H_2O$. Each Tb atom is nonacoordinated by the four nitrogen atoms of a ligand, three O atoms from the phosphonate functions of the ligands, one water molecule and an O atom of a phosphonate function of the neighboring TbL complex.

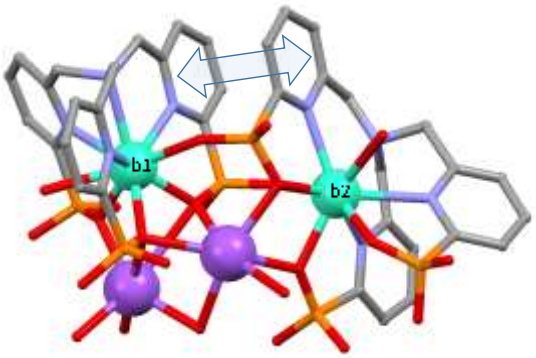

Figure 4. X-ray crystal structure of the Tb complex (H atoms have been omitted for the sake of clarity, Tb, green; Na, violet; C, grey; N, blue; O, red; P, orange, the double arrow represents the inter-complex π-π stacking interaction).

The two TbL complexes are stabilized by a π-π stacking interactions between two pyridyl rings denoted by a double arrow in Figure 4, with a centroid to centroid distance of 3.507 Å within the rings. In a TbL complex, the O atom making the bridge with the second TbL complex is not directly coordinated to its Tb atom, but belongs to the phosphonate moiety of the pyridyl rings involved in the stacking interaction.

Table 2. Main characteristics of the [LnL] complexes in the solid state.

		CN	Average negative charge per complex (per ligand)	$d_{Ln\text{-}O(P)\ av.}$ (Å)	$d_{Ln\text{-}Owater}$ (Å)	$d_{Ln\text{-}Ntert\ av.}$ (Å)	$d_{O\text{-}O\ av.}$ [a] (Å)
Eu [10]	Dimer	9	- 1.75	2.384	2.646 [b]	2.693	3.037
			(- 4.75)		2.870 [c]		
Gd	Monomer	8	- 3	2.313	2.460	2.691	3.050
		(9) [d]	(-6)	(2.432) [d]	(2.586) [d]	(2.829) [d]	(3.206)
Tb	Dimer	9	- 1	2.360	2.600	2.639	2.920
			(- 4)				

[a] Average distances between the coordinated oxygen atoms of the phosphonate functions. [b] Terminal Eu-OH_2 bond (see text). [c] The O atom of the Eu-OH_2 bond is bridging a Na^+ cation (see text). [d] Values calculated for a CN of 9 assuming an increase of the ionic radius from 1.053 Å (CN = 8) to 1.107 Å (CN = 9) according to reference 21.

Table 2 summarizes some of the main characteristics of the LnL complexes (Ln = Gd and Tb, this work, Ln = Eu reference 10). Considering that the refinement process of the structures introduces the possible squeezing of some H atoms of the water molecules, some hydroxide anions may be hidden by the fitting procedure and it is quite difficult to ascertain the charge of the complexes. This charge was thus arbitrarily calculated from the number of sodium ions found in the structure to counterbalance the charge of the complexes, explaining the non-integer value reported for the Eu complex, with the unit cell containing 4 Eu^{3+}, 4 ligands and 7 Na^+ cations (which corresponds to a formula: {[(EuLH_2(H_2O)]Na} {[(EuLH(H_2O)] Na_2}.($H_2O)_{12}$). The Eu complex also possesses the particularity to display two very different kinds of bonds for the water molecule linked to the EuL complexes. The shortest bond (2.646 Å) is a terminal Eu-OH_2 bond, whereas in the second and largest one (2.870 Å), the oxygen atom of the water molecule is bridging the Eu atom and a Na^+ cation. Notably, for the lighter Eu atom, the coordination number (CN) is 9, as for Tb, whereas it decreased to 8 for Gd. Considering this change in CN, and for the sake of comparison between the structures, values in parenthesis were given for the Gd complex corresponding to distances calculated for a CN of 9 assuming an increase of the ionic radii from 1.053 Å to 1.107 Å for Gd with CN of 8 and 9 respectively.[21]

From the results of Table 2, it unfortunately appears to be very difficult to identify clear trends that would link the charges (and indirectly the protonation state of the ligands) and the different distances, especially in view of the change in CN on the one hand and of the presence of monomer or dimers on the other hand. However, the comparison between the complexes reveals quite interesting features. It seems that the average distances between the Ln cation and the coordinated oxygen atoms of the phosphonate functions ($d_{Ln\text{-}O(P)\ av.}$) are very close whatever the complexes and their charges with less than 8 ppm deviations, considering or not the change in the CN. Regarding the water molecule not coordinated to a Na^+ cation for Eu and the correction for the different CN for Gd, it similarly appears that the distances between the Ln cation and the oxygen atom of the coordinated water molecule ($d_{Ln\text{-}Owater}$) are very similar, within 6 pm. The most striking differences arise from the comparison of the distances between the Ln cations and the apical tertiary nitrogen atom of the ligand ($d_{Ln\text{-}Ntert\ av.}$). While the increase of the negative charge of the complex from Tb (-1) to Eu (-1.75) has a minor influence, especially if one takes into account the correction for the lanthanide contraction,[22] the full deprotonation of the ligand in the Gd complex resulted in a marked lengthening of this distance, compensated by the decrease of the CN for Gd. The full deprotonation of the ligand results in a displacement of the cation towards the phosphonate functions in the cavity of the tripodal ligand. A final aspect of this comparison is revealed by the average distances between the coordinated oxygen atoms of the phosphonate functions, which occupy adjacent positions in the coordination polyhedron. Here again, the increase of the negative charge from Tb to Eu results in a small increase of this distance, but almost negligible if one account for the increase of the ionic radius of Eu^{3+} (the correction would lead to a distance of 2.987 Å for Tb). However, one can notice a net increase of the O-O distances for Gd (3.050 Å), which becomes evident if one compares the lengths for a same CN of 9 (3.206 Å), and reaching 3.244 Å if normalized to the ionic radius of Eu^{3+}.

^{1}H relaxivity and ^{17}O NMR studies of GdL. Relaxivity (r_1) of a dilute aqueous solution of the Gd-complex, [GdL], at neutral pH (pH=7.2) and at the temperature of 298 K assumes the value of 8.9 mM^{-1} s^{-1}. This value is significantly greater than those of monohydrated Gd^{III} complexes of similar molecular size.[2b] On the other hand, the relaxivity is not high enough to suggest a higher state of hydration (q > 1). The variation of the longitudinal relaxation rate as a function of pH for the [GdL] complex over the range 11–2 (at 20 MHz and 298 K, Figure 5) was investigated to assess the possible presence of changes in the hydration number and self-association or hydrolysis processes. The water proton relaxivity shows a constant value of *ca.* 10.6 mM^{-1} s^{-1} from pH 2 up to pH ~6 and then it markedly decreases to reach a new plateau at pH > 8.5, where r_1 has the value of 6.2 mM^{-1} s^{-1}. The inflection point of the sigmoidal curve can be estimated to correspond to a pH value of 7.4, which could be associated with a protonation step. The variation of r_1 between the basic and acid region, Δr_1, is approximately equal to 4.4 mM^{-1} s^{-1}, a value that corresponds rather well to the increase in relaxivity that follows a change in the hydration number from 1 to 2. In fact, a Δr_1 of 6.4 mM^{-1} s^{-1}, associated with a change of q of 1.4, has been reported recently.[23] Overall, these results reproduce quite well the pH-dependent variation in relaxivity previously observed in other systems.[24]

To get further insight into the physico-chemical properties of this novel Gd(III) complex and into its pH-dependent relaxivity, ^{1}H and ^{17}O NMR relaxometric studies as a function of magnetic field strength and temperature were performed. The measurement of the relaxivity as a function of the proton Larmor frequency (or magnetic field strength) provides a series of data known as the nuclear magnetic relaxation dispersion (NMRD) profile. The analysis of such profiles based on the established theory of paramagnetic relaxation[25] makes it possible to assess the values of several structural, electronic and dynamic parameters of the paramagnetic complex, including the number of water molecules in the inner-coordination sphere (q), their distance from the paramagnetic center (r) and the overall molecular tumbling time of the complex (τ_R). In addition, the variation of the ^{17}O NMR transverse relaxation rate (R_2) and shift ($\Delta\omega$) values as a function of temperature provides accurate information on the kinetics of exchange of the bound water ($k_{ex} = 1/\tau_m$). [25] The experimental profiles were obtained at 283, 298 and 310 K at both pH = 9.8 and 4.7, over the frequency range 0.01 to 70 MHz (Figure 6). The shape of the NMRD profiles and their temperature dependence (r_1 decreases with increasing temperature) reproduce the general behavior of small Gd^{III} complexes, characterized by a plateau at low fields, a dispersion around 4–8 MHz and another region at high fields (> 20 MHz) where r_1, at room temperature or higher, shows only very little changes. At 283 K, the relaxivity shows a tendency to increase at high field (>20 MHz) with formation of a broad hump centered about 60 MHz.

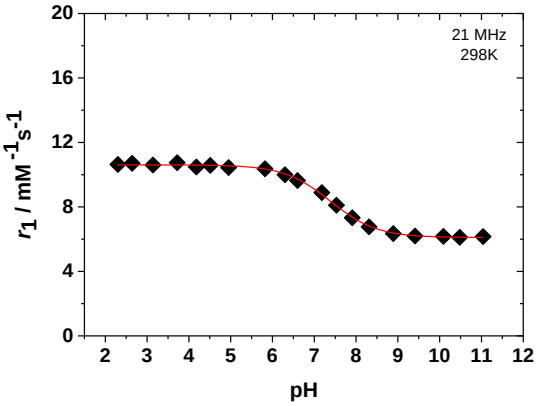

Figure 5. pH dependency of the longitudinal relaxivity of [GdL] at 298 K and 0.5 T.

The lower values of the relaxivity with increasing temperature, over the entire range of proton Larmor frequencies investigated, indicate that r_1 is not limited by the water exchange rate (*fast exchange* regime) but rather by the rotational motion, as for the related monomeric complexes. This general trend is valid for NMRD profiles measured both at acid and basic pH. These differ simply in their amplitude, suggesting that the variation is associated with a non-frequency dependent parameter, such as the hydration number q. It is therefore reasonable to assume a value of q = 1 for the complex in the basic region and q = 2 in the acid region.

A least-square fit of the ^{1}H NMRD data was carried out using the standard theory of paramagnetic relaxation expressed by the Solomon-Bloembergen-Morgan (SBM),[26] for the inner-sphere (IS) contribution, and Freed's equations,[27] for the outer sphere (OS) relaxation mechanism. Considering the high number of parameters requiring fitting, some of them were fixed at known or reasonable values. The hydration number q was fixed to 1 at pH 9 and to 2 at pH 4.7; the distance between Gd^{3+} and the protons of the bound water molecule, r, was fixed to 3.0 Å; the distance of closest approach, a, of the outer sphere water molecules to Gd^{3+} was set to 4.0 Å and for the relative diffusion coefficient D standard values of 1.30, 2.24 and 3.1×10−5 cm^2 s^{-1} (283, 298 and 310 K) were used. The fit was performed using as adjustable parameters the rotational correlation time, τ_R, and the electronic relaxation parameters Δ^2 (trace of the squared zero-field splitting, ZFS, tensor) and τ_V (correlation time for the modulation of the transient ZFS). The best-fit parameters are listed in Table 3 and compared with those of related Gd(III) macrocyclic complexes of similar sizes with q = 1 and 2. The experimental NMRD profiles are well reproduced with the set of best-fit parameters, which clearly show that the r_1 of [GdL] is dominated by the rotational dynamics and that its pH dependence may be attributed predominantly to an increase of the hydration state on passing from basic to acid regions.

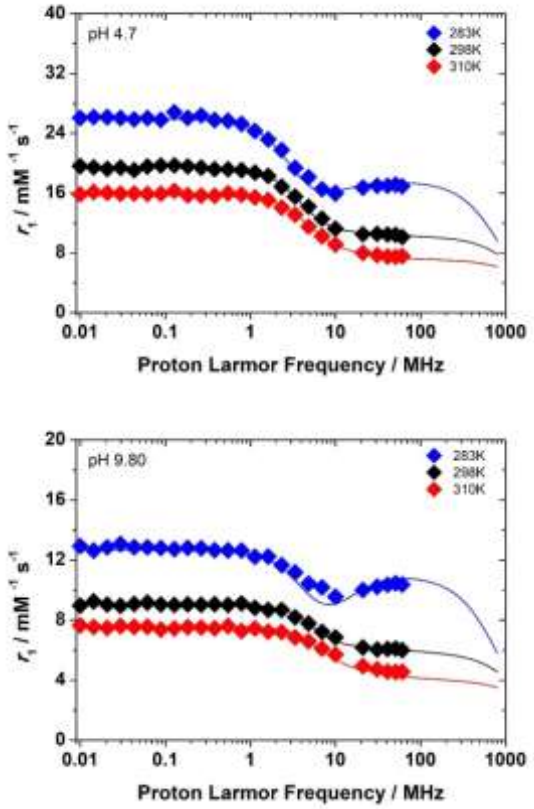

Figure 6. $1/T_1$ ^{1}H NMRD profiles of [GdL] at 283, 298 and 310 K at pH 4.7 (top) and pH 9.8 (bottom).

Variable temperature reduced transverse ^{17}O NMR relaxation rates (R_{2r}) and chemical shifts ($\Delta\omega_r$) were recorded at 11.7 T on a 15 mM solution of the Gd complex in ^{17}O-enriched water. The data were analysed using Swift-Connick set of equations that provide accurate estimates of the water exchange lifetime, τ_M. The experimental temperature dependencies of R_{2r} ($1/T_{2r}$) and $\Delta\omega_r$ values are reported in Figure 7. The $1/T_{2r}$ values increase with the decrease in temperature over a wide range of values to indicate the occurrence of a fast water exchange rate both under acidic and basic conditions. This result is in full agreement with the temperature dependency of the NMRD profiles. ^{17}O NMR R_2 data primarily depend on the electronic relaxation times (described by the parameters Δ^2 and τ_V), on the hyperfine Gd-$^{17}O_{water}$ coupling constant ($A_O/\hbar$), on τ_M and on q. Information on q and $A_O/\hbar$ are derived from the variation of $\Delta\omega_r$ with temperature. Additional parameters associated with the exchange process are the exchange lifetime of the coordinated water molecule(s), τ_M, and its enthalpy of activation, $\Delta H_M^{\#}$. The activation energy for the modulation of the zero-field splitting interaction (E_v) and the rotational motion of the complex (E_R), were fixed to the standard values of 1.0 and 16 kJ·mol^{-1}, respectively. The best-fit parameters are reported in Table 3.

The water exchange rate is very high at both pH values and more than 2 orders of magnitude faster than for the clinical MRI probes GdDTPA and GdDOTA.[25] This could be the consequence of a pronounced degree of steric compression around the bound water molecule induced by the bulky phosphonate groups, as previously reported for other phosphonated complexes such as GdEGT1P (k_{ex} = 41.7×10^7 s^{-1}),[28] and GdDO3AP (k_{ex} = 71.4×10^7 s^{-1})[29] and complexes containing both pyridine and phosphonate groups.[30]

The values obtained for the ^{17}O hyperfine coupling constants are in the range typically observed for Gd^{3+} complexes ($A_O/\hbar \approx$ -2.5× 10^6 to -4.0 × 10^6 rad s^{-1}). The relatively small value of $A_O/\hbar$ for GdL in basic conditions has been previously observed and explained in terms of an efficient spin delocalization on the ligand backbone caused by the presence of aromatic units.[31] The small value could be also associated with a slightly longer Gd-O_{water} distance.

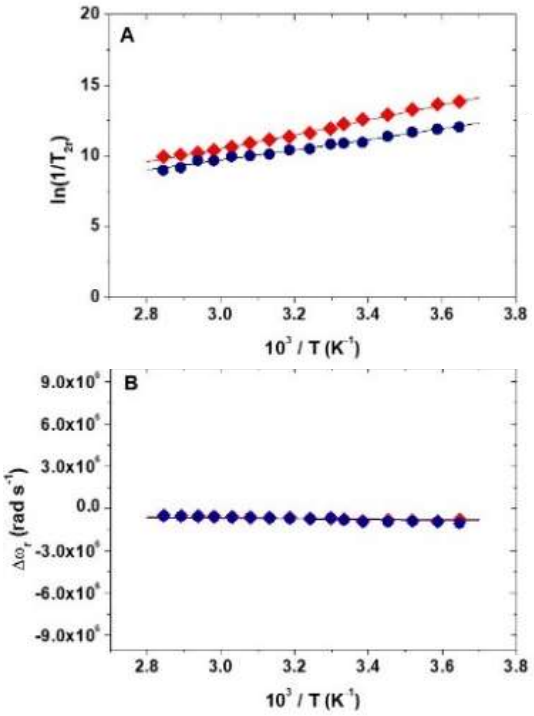

Figure 7. Reduced ^{17}O NMR transverse relaxation rates (T_{2r}, top) and ^{17}O NMR chemical shifts ($\Delta\omega_r$, bottom) as a function of temperature for [GdL] measured at 67.8 MHz (11.74 T) and at pH 4.7 (red) and pH 9.8 (blue). The solid lines were calculated using the parameters listed in Table 3.

Concerning the parameters related to the electron spin relaxation of the metal ion (Δ^2 and τ_V), the parameters obtained from the analysis of NMRD and ^{17}O NMR data are similar to those obtained for other Gd^{3+} complexes such as GdDTPA-BMA, GdDTPA and GdDOTA.[32]

Table 3: Relaxometric parameters obtained by the simultaneous analysis of ^{1}H NMRD profiles and ^{17}O NMR data (11.7 T) for the GdL complex at basic and acid pH.

	pH = 9.8 [a]	pH = 4.7 [a]
$^{60}r_1^{298}$ ($mM^{-1}s^{-1}$)	6.0	10.1
Δ^2 / 10^{19} s^{-2}	3.8 ± 0.2	2.0 ± 0.1
τ_V^{298} / ps	28 ± 2	30 ± 2
$^{298}k_{ex}$ / 10^7 s^{-1}	89.3 ± 3.6	33.3 ± 1.1
ΔH_M / *k*J mol^{-1}	34.8 ± 1.4	44.1 ± 0.9
τ_R^{298} / ps	110 ± 3	111 ± 2
$A_O/\hbar$ / 10^6 rad s^{-1}	-2.6 ± 0.2	-3.5 ± 0.1
q	1[b]	2[b]
r / Å	3.0 [b]	3.0 [b]

[a] Values of 16.0 and 1.0 kJ mol^{-1} were used and for the parameters E_R, and E_V, respectively; [b] fixed in the fitting procedure.

Luminescence spectroscopy of the Eu complex. Considering the previous results obtained on the relaxivity of the Gd complex, it appeared of interest to have a deeper look at the luminescence properties of the Eu analogue in solution, assuming that the behavior of both complexes are the same in solution. Since the pioneering works of Horrocks and co-workers[33] and their refinement by Parker *et al*,[34] it is well established that the luminescence lifetime of Eu complexes is strongly related to their hydration states *q* with the relationship:

$$q = A\left(\frac{1}{\tau_{H2O}} - \frac{1}{\tau_{D2O}} - a\right) \qquad (1)$$

In which τ represents the luminescence lifetime in H_2O or D_2O, *A* and *a* being constants for a specific Ln cation (*A* = 1.2 ms and *a* = -0.25 ms^{-1} for Eu).[34] We thus hypothesized that, assuming that the Eu and Gd complexes are isostructural in solution, the measurement of the luminescence lifetime at different pH and pD values[35] would allow us to corroborate the assumption of a decreased *q* value at basic pH. Figure S7 and S7 represent the Eu excited state lifetimes as a function of pH and pD, respectively, and Figure 8 represents the evolution of the measured luminescence lifetimes of the Eu complex as a function of the pH in water and in deuterated water, as well as the *q* values determined with these titrations.

In pure water, the luminescence lifetime first decreased from 450 to 280 µs from pH 2 to 3, is almost constant up to pH 5 and finally displayed a constant increase up to pH 9 at which it leveled off at almost 600 µs. In D_2O, a similar decrease is observed from pD 2 to pD 3, the lifetime is then constant up to pD 8 and finally dropped. Considering these data, the measured *q* values were found to be close to 2 at acidic pH and showed a drop to 1 at pH close to 8. These results are in perfect agreement with those previously obtained by relaxometry measurements on the Gd complex.

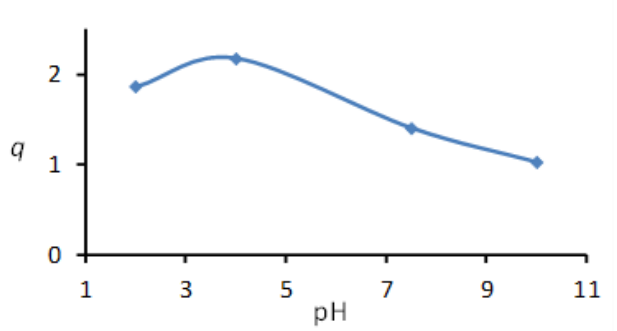

Figure 8. Calculated hydration number obtained for the EuL complex using equation 1 (estimated error of ± 0.2 water molecules).[34]

These combined NMR and luminescence data suggest that the hydration state of the complexes is changing, decreasing from two to one upon basification. Considering that the Eu complex was found to be a dimer in the solid state with *q* = 1, a putative explanation of the phenomenon may be associated with a pH dependent monomer-dimer equilibrium. In such equilibrium, acidification would result in the dissociation of the dimer leading to the disruption of the bond between one Eu complex and the bridging bond formed with the phosphonate function of the second complex according to Scheme 2.

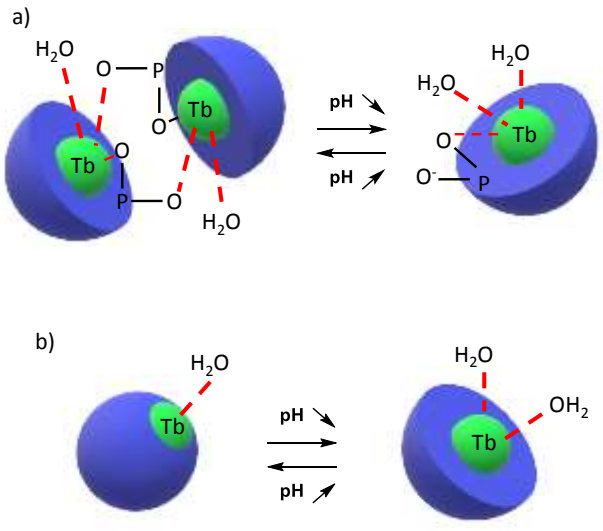

Scheme 2. Possible mechanisms for the pH induced hydration change: a) Monomer/dimer equilibrium; b) breathing motion of the ligand.

A second hypothesis arose from a kind of breathing mode of the complex. At acidic pH values, the phosphonate functions are found as monoprotonated (R-P(O)(OH)O$^-$), decreasing the interaction between the Ln cation and the coordinating oxygen atom and increasing the overall positive charge of the complex. The corresponding distance is long enough to leave the place for two water molecules in the first coordination sphere with a CN of 9. Upon increase of the pH, the phosphonate functions gradually lose their protons leading to doubly charged phosphonate functions (R-P(O)(O$^-$)$_2$) resulting in stronger electrostatic interactions between the coordinated O atoms and the Ln cation and thus shorter Ln-O bonds. The ligand is contracted around the metal and the remaining void space occupied by solvent molecules decreased, leading to the expulsion of one of the two water molecules. The overall increased negative charge of the complex is also expected to disfavor the coordination of water molecules due to electrostatic reasons.

In order to investigate the potential formation of aggregates in solution, diffusion ordered spectroscopy (DOSY) measurements were performed on solutions of the diamagnetic Lu complex. The ^{1}H NMR spectra recorded at pD values of 4.5 and 10.4 in D_2O (298 K, 5 mM) are consistent with the presence of a single major species in solution (Figure S9, Supporting Information) that provides self-diffusion coefficients of 3.3×10^{-10} and 3.0×10^{-10} m^2 s^{-1} at pD 4.5 and 10.4, respectively. These values are very similar to those reported for mononuclear La and Lu complexes with similar molecular weight,[36] but higher than the self-diffusion coefficients measured for dimeric or trimeric entities.[37] The slightly lower diffusion coefficient measured at pD 9.5 can be attributed to a larger hydrodynamic radius of the complex associated to an increased negative charge. Thus, we conclude that the [LuL] complex does not experience significant aggregation in solution, confirming that the relaxivity change observed with pH is related to a change in the hydration number of the monomeric complex.

NMR studies. The paramagnetic shifts induced by Yb^{3+} are dominated by the pseudocontact contributions, which are related to the magnetic anisotropy of the complex and the location of the observed nuclei with respect to the principal magnetic axes.[38] The pseudocontact shifts of Yb^{3+} and other lanthanide complexes were found to be very sensitive to small structural changes,[39] for example induced by changing the polarity of the solvent.[40] Thus, we sought to investigate the ^{1}H and ^{31}P NMR spectra of the YbL complex at different pH (pD) values. The ^{1}H spectrum of YbL recorded at pD 11.5 presents three relatively sharp peaks due to the proton nuclei of the pyridyl ring at 16.8, 10.6 and 2.5 ppm, and a broader signal attributed to ligand CH_2 protons at -27.4 ppm (Figure 9). Lowering the pH provokes a very important shift of the signal at -27.4 ppm, which is observed at -5.9 ppm at pH 4.5. The signals of the pyridyl protons also experience important chemical shifts (Figure 9). Similarly, the ^{31}P NMR spectrum recorded at pD 11.5 presents a single signal at 46.6 ppm that experience a large upfield shift as the pD is lowered, reaching a value of 11.9 ppm at pD 3.9. These spectral changes clearly evidence an important change of the magnetic anisotropy of the complex upon lowering the pH, which must be related to an important structural change occurring in solution.[41] The chemical shift data provided an apparent pK_a value of 5.44(3).

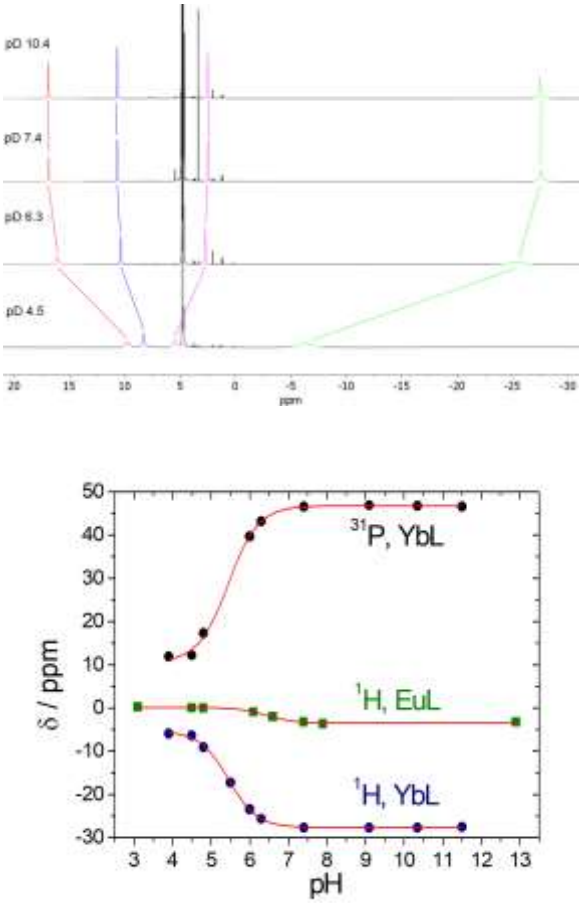

Figure 9. Top: ^{1}H NMR spectra (500 MHz, D_2O, [c] = 1.65×10^{-2} M) recorded for the YbL complex at different pD values. Bottom: Variation with pD of the chemical shifts of the ^{1}H CH_2 proton signal of EuL and YbL and the ^{31}P signal of YbL.

The ^{1}H NMR spectrum of the EuL complex shows similar pH-dependent changes, though less pronounced. The signal of the ligand CH_2 protons, which is observed at -3.2 ppm at pH 12.9, experiences a downfield shift below pH ~ 8 reaching δ = 0.3 at pH 3.1. Conversely, the chemical shift of the ^{31}P NMR signal shows little changes with pH. The ^{1}H NMR data provide an apparent pK_a of 6.4, which is ~0.8 units lower than the first protonation constant of the complex determined from potentiometric titrations. This discrepancy is likely related to the different concentration ranges used in the two sets of experiments and the different ionic strengths. Nevertheless, the NMR data clearly support an important structural change

occurring in solution, in nice agreement with the results obtained from luminescence and ^{1}H relaxometry. This structural change appears to take place at considerably lower pH in the case of the Yb^{3+} complex compared to the Gd^{3+} and Eu^{3+} analogues.

DFT calculations. A DFT study was carried out to gain information of the structural changes induced by pH at the molecular level. On the grounds of previous investigations, we employed a mixed continuum-explicit approach in which bulk solvent effects are considered with a polarized continuum model (PCM), while a number of second-sphere water molecules are explicitly included to provide an accurate description of the Gd-O_{water} distances, and spin densities at the nuclei of the coordinated water molecules. Previous calculations showed that the explicit inclusion of two second-sphere water molecules involved in hydrogen bonds with each coordinated water molecule was enough to obtain accurate Gd-O_{water} distances and ^{17}O hyperfine coupling constants.[42,43] Thus, we performed geometry optimizations of the $[GdL(H_2O)_2]^{3-}\cdot 4H_2O$, $[GdHL(H_2O)_2]^{2-}\cdot 4H_2O$ and $[GdH_2L(H_2O)_2]^{-}\cdot 4H_2O$ systems (Figure 10), which contain two coordinated water molecules and four additional second-sphere water molecules. Subsequently we explored the potential energy surface by enlarging one of the Gd-O_{water} distances, which yielded a new set of energy minima containing a single coordinated water molecule.

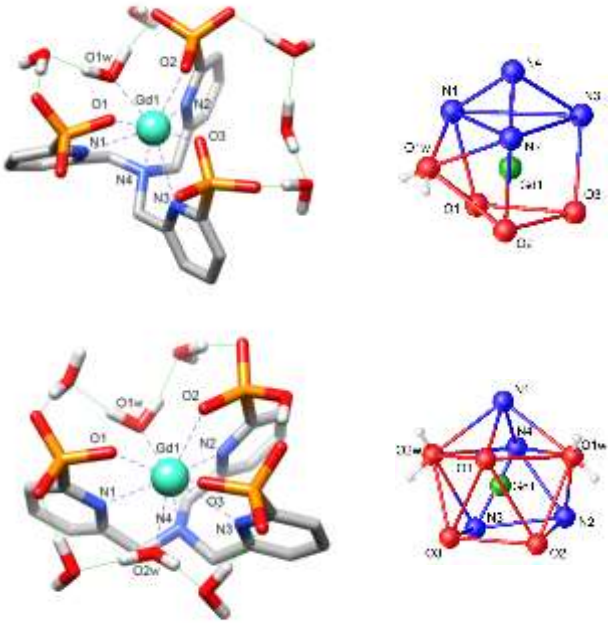

Figure 10. Views of the structures obtained with DFT calculations for the $[GdL(H_2O)]^{3-}\cdot 5H_2O$ (top) and $[GdHL(H_2O)_2]^{2-}\cdot 4H_2O$ (bottom) systems and the corresponding coordination polyhedra.

The energy difference between the $[GdL(H_2O)_2]^{3-}\cdot 4H_2O$ and $[GdL(H_2O)]^{3-}\cdot 5H_2O$ species favor the latter by ΔE_{ZPE} = 1.78 kcal mol^{-1}. This situation is reversed upon protonation of one of the phosphonate groups, so that the bis-hydrated complex is more stable by 0.45 kcal mol^{-1}. Protonation of a second phosphonate function provides an additional stabilization of the q = 2 form of the complex over that with q = 1 (ΔE_{ZPE} = 0.96 kcal mol^{-1}). Thus, the results obtained with DFT are in perfect agreement with both the luminescence and relaxometric data.

Complex protonation causes important changes in the structure of the complex besides the increased number of coordinated water molecules. Indeed, in the $[GdL(H_2O)]^{3-}\cdot 5H_2O$ system the three pyridyl rings of the ligand are folded in the same direction with respect to the axis containing the pivotal N atom and the Gd^{3+} ion. As a result, the three chelates rings involving the pivotal N atom and the N atoms of the pyridyl rings adopt identical conformations (δ or λ).[44] The overall conformation of the complex can thus be denoted as (δδδ) and that of the mirror image (λλλ). In contrast, the orientation of two of the pyridyl units in $[GdHL(H_2O)_2]^{2-}\cdot 4H_2O$ is opposite to the third, leading to an overall (δλλ) [or (λδδ)] conformation (Figure 10). This conformation is likely stabilized by the presence of an intramolecular hydrogen bond involving the protonated phosphonate group and an oxygen atom of a neighboring phosphonate and is fully consistent with the conformations observed for the fully deprotonated Gd complex, compared to the partially protonated structures of the Eu and Tb complexes (Figure 11).

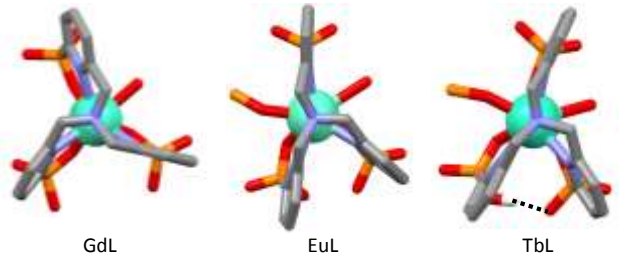

Figure 11. Views of the X-ray crystal structures of the Gd (a), Eu (b) and Tb (c) complexes along the Ln-$N_{tert.}$ bond, showing the (*δδδ*) (a) and (*λδδ*) (b and c) conformations of the ligands (the supplementary coordination of the Eu and Tb complexes is highlighted by the presence of the P atom of the second complex in the dimers). H atoms have been removed for the sake of clarity, except for the TbL complex, in which the H bonding interactions joining the two arms has been added (H atoms were not refined in the case of the Eu structure).

The different ligand conformation and hydration number in the $[GdL(H_2O)]^{3-}\cdot 5H_2O$ and $[GdHL(H_2O)_2]^{2-}\cdot 4H_2O$ complexes result in different coordination polyhedra. In $[GdL(H_2O)]^{3-}\cdot 5H_2O$ the coordination polyhedron can be best described as a trigonal prism defined by the three N atoms of the pyridyl units and the three oxygen atoms of the phosphonate groups coordinated to the metal ion. The pivotal N atom (N4) is capping the face delineated by the pyridyl N atoms, while the coordinated water molecule is capping one of the quadrangular faces of the

polyhedron. In contrast, the coordination polyhedron in $[GdHL(H_2O)_2]^{2-}\cdot 4H_2O$ can be viewed as a capped square antiprism, where the nitrogen atom of the pyridyl unit N1 occupies the capping position. The calculated bond distances of the metal coordination environments are provided in Table S2 (Supporting Information).

The structure of the Yb complex in solution was further investigated by analyzed the Yb-induced paramagnetic shifts, which are largely dominated by the pseudocontact contribution. For axially symmetric systems, the pseudocontact shifts can be expressed as:[38]

$$\delta^{pc} = D_1 \frac{3cos^2\theta - 1}{r^3} \qquad (2)$$

Where *r* is the distance between the observed nucleus and the Yb ion, θ is the angle defined by the H-Yb vector and the principal magnetic axis of the complex and D_1 is proportional to the axial magnetic anisotropy of the system. The ^{1}H NMR spectra recorded for the Yb complex evidence an effective C_3 symmetry of the complex in solution. Thus, we estimated the geometric factor in Eq (2) using the DFT calculated structures by assuming that the principal magnetic axis coincides with the Ln-N_{tert} vector (N_{tert} is the tertiary N atom of the ligand). Subsequently, the geometric factors where plotted against the observed paramagnetic shifts, using the chemical shifts of the Lu analogue to estimate the diamagnetic contributions (Table S3, Supporting Information). These plots provided a straight lines passing through the origin (R^2> 0.996) with slopes of D_1 = -1628 ± 35 and -534 ± 36 at pH 10.4 and 3.9, respectively (Figure S10, Supporting Information). These results indicate that our DFT calculations provide a good description of the structure of the complexes in solution, and confirm that the structural change triggered by changing the pH provokes a dramatic change of the magnetic anisotropy of the complex.

DFT calculations were used to compute the hyperfine coupling constants $A/\hbar$ that determine the ^{17}O chemical shifts and transverse relaxation rates. The $A/\hbar$ values determined for Gd^{3+} complexes generally fall within a rather narrow range of -3.0 × 10^6 to -4.0 × 10^6 rad s^{-1}.[45] As a result, ^{17}O NMR measurements can provide a reliable measure of the hydration state of Gd^{3+} complexes. The $A/\hbar$ value determined for the Gd^{3+} complex of L at pH 9.8 (-2.6 × 10^6 rad s^{-1}), where the $[GdL(H_2O)]^{3-}$ species largely predominates, falls clearly below the normal range. However, at pH 4.7 the $A/\hbar$ value obtained from NMR measurements is within the range normally observed for Gd^{3+} complexes. At this pH value the complex presents significant populations of the protonated $[GdHL(H_2O)_2]^{2-}$ and $[GdH_2L(H_2O)_2]^{-}$ species. The hyperfine coupling constant calculated for the $[GdL(H_2O)]^{3-}\cdot 5H_2O$ system with DFT calculations is -1.9 × 10^6 rad s^{-1}, in reasonably good agreement with the experimental value. This low absolute value of $A/\hbar$ is likely related to the long calculated Gd-O_{water} distance (2.530 Å), as computational studies revealed that $A/\hbar$ is very sensitive to this parameter.[42] For $[GdHL(H_2O)_2]^{2-}$ our calculations provide two rather different Gd-O_{water} distances of 2.552 and 2.497 Å, corresponding to $A/\hbar$ values of -2.3 × 10^6 and -2.9 × 10^6 rad s^{-1}, respectively. The average value of $A/\hbar$ obtained for $[GdHL(H_2O)_2]^{2-}$ (-2.6 × 10^6 rad s^{-1}) is clearly higher (in absolute terms) than that obtained for $[GdL(H_2O)]^{3-}$ (-1.9 × 10^6 rad s^{-1}). Thus, while our calculations appear to underestimate $A/\hbar$ by about 25%, the results do support the unusually low value of $A/\hbar$ determined from ^{17}O NMR for $[GdL(H_2O)]^{3-}$.

The electronic ^{8}S ground state of Gd^{3+} ion is characterized by an electronic spin state S = 7/2, which implies that the degeneracy of the magnetic sublevels M_S = ± 7/2, ± 5/2, ± 3/2 and ± 1/2 is broken in the absence of any applied magnetic field due to zero-field splitting effects. An interesting feature revealed by the fits of the ^{1}H NMRD profiles is the rather different values of the square of the zero-field splitting energy determined at pH 9.8 and 4.7 (Table 3). We thus performed calculations of the ZFS parameters of the $[GdL(H_2O)]^{3-}\cdot 5H_2O$ and $[GdHL(H_2O)_2]^{2-}\cdot 4H_2O$ systems. DFT methods were found to be quite unreliable to predict the ZFS parameters of Gd^{3+} and Mn^{2+} complexes, while *ab initio* calculations based on CASSCF wave functions were found to provide better results.[46] We thus performed CASSF/NEVPT2/QDPT calculations, which yielded the axial (*D*) and rhombic (*E*) ZFS parameters shown in Table 4. The *D* parameters differ both in sign and magnitude, a situation that reflects the different splitting of the Kramer doublets of the octet ground state (Figure S11, Supporting Information). The ZFS energy can be calculated from the values of the axial and rhombic ZFS parameters as follows:

$$\Delta = \sqrt{\frac{2}{3}D^2 + 2E^2} \qquad (3)$$

The values of Δ^2 obtained with calculations present an excellent agreement with the experimental values obtained with NMR measurements. It is important to note that the electron spin relaxation times present contribution of transient distortions of the ZFS (transient ZFS) and the average ZFS in the molecular frame (static ZFS).[47] Thus, our calculations have to be taken with some care, as dynamic effects were not considered. However, they support that the structural change induced by the protonation of the complex provokes an important variation of the ZFS, as suggested by NMRD studies.

Table 4. ZFS parameters obtained with CASSCF/NEVPT2/QDPT calculations.

	D/cm^{-1}	E/D	Δ/cm^{-1}	Δ^2 10^{19}rad^{2}s^{-2}
$[GdL(H_2O)]^{3-}\cdot 5H_2O$	-0.042	0.122	0.034	4.1
$[GdHL(H_2O)_2]^{2-}\cdot 4H_2O$	0.029	0.243	0.026	2.4

Conclusion

The podand type ligand L forms very stable LnL complexes in solution as evidenced by potentiometry and spectrophotometric measurements. Upon protonation, the $[LnL]^{3-}$ complexes display a remarkable change in the conformation of the ligand in which the three pyridyl strands initially display a $\delta\delta\delta$ (or $\lambda\lambda\lambda$) conformation rearrange into a ($\delta\delta\lambda$) (or $\delta\lambda\delta$ or $\delta\lambda\lambda$) one, the additional proton bridging two phosphonate functions of the ligand. This simple reorientation of one of the pyridyl arms results in a steric release around the Ln cation with the concomitant entrance of a second water molecule in the first coordination sphere of the cation. This change of hydration is translated into drastic changes of the magnetic and spectroscopic properties of the complexes as evidenced by the doubling of the r_1 relaxivity of the Gd complex with a pK of 7.24, of potential interest for biological processes. Such a behavior was previously observed for some DOTA derivatives bearing a sulfonamide pendant arm in which the increase of the pH led to deprotonation of the sulfonamide function and coordination of the deprotonated N atom of the amide, engendering the removal of two water molecules from the first coordination sphere of the Gd atom.[48] Alternatively, the change in hydration can also be the result of the ligation of the Gd contrast agents with proteins,[49] or with endogeneous anions,[50] such hydrogenocarbonates and phosphates, although in that case it generally results in a drop of the relaxivity. In the present case, the deprotonation is not accompanied by any change in the coordination mode of the ligand, but only by a subtle rearrangement opening the place for the entrance of the second water molecule.

Experimental Section

Eu, Tb and Yb complexes were synthesized according to literature procedures.[10] Full experimental details concerning the synthesis of the Gd and Lu complexes, potentiometric and spectrophotometri studies, crystallography, DFT and Ab Initio calculations and NMR measurements can be found in the Supporting information section, with additional data concerning UV-Vis spectra of L; ES/MS characterization of GdL; stacking interactions in GdL; Evolution of the lifetime of the Eu complex in H_2O and D_2O as a function of pH (pD); 2D-DOSY spectra of LuL at different pH; plot of the observed paramagnetic shift of YbL and splitting of the Kramer's doublet in GdL (10 Figures); Crystal data and structure refinement for the TbL and GdL complexes; Calculated bond distances (Å) of the metal coordination environments of the Gd; ^1H and ^{31}P NMR shifts (ppm) for YbL and LuL complexes; Optimized Cartesian coordinates of $[GdL(H_2O)]^{3-}\cdot 5H_2O$ and $[GdHL(H_2O)_2]^{2-}\cdot 4H_2O$ obtained with DFT calculations (5 Tables).

Acknowledgements

C.C. gratefully acknowledged the French National Research Agency (ANR) for financial support (Neutrinos project n°16-CE09-0015-02). M.B. is grateful to MIUR for financial support (Grant n° 2017A2KEPL_002; PRIN 2017). C. P.-I. D. E.-G. and I. B. acknowledge Xunta de Galicia (ED431B 2017/59) for generous financial support.

Keywords: Gadolinium • contrast agent • MRI • hydration • relaxivity

[1] a) E. Boros, E.M. Gale, P. Caravan, *Dalton Trans.* **2015**, *44*, 4804-4818. b) J. Wahsner, E.M. Gale, A. Rodríguez-Rodríguez, P. Caravan, *Chem. Rev*. **2019**, *119*, 957−1057.

[2] a) E. Tóth, C. Bonnet, *Inorganics*, **2019**, *7*, 68. b) E.M. Gale, I. Atanasova, F. Blasi, I. Ay, P. Caravan, *J. Am. Chem. Soc.* **2015**, *137*, 15548-15557; c) R. Pujales-Paradela, T. Savic, I. Brandariz, P. Perez-Lourido, G. Angelovski, D. Esteban-Gomez, C. Platas-Iglesias, *Chem. Commun.* **2019**, *55*, 4115-4118.

[3] R. Pujales-Paradela, F. Carniato, D. Esteban-Gomez, M. Botta, C. Platas-Iglesias, *Dalton Trans*. **2019**, *48*, 3962-3972.

[4] a) K.H. Chalmers, E. De Luca, N.H.M. Hogg, A.M. Kenwright, I. Kuprov, D. Parker, M. Botta, J.I. Wilson, A.M. Blamire, *Chem. Eur. J.* **2010**, *16*, 134-148. b) K.H. Chalmers, M. Botta, D. Parker, *Dalton Trans.* **2011**, *40*, 904-913. c) K. Srivastava, E.A. Weitz, K.L. Peterson, M. Marjanska, V.C. Pierre, *Inorg. Chem.* **2017**, *56*, 1546−1557. d) J. Blahut, P. Hermann, A. Gálisová, V. Herynek, I. Císařová, Z. Tošnerc, J. Kotek, *Dalton Trans.* **2016**, *45*, 474-478.

[5] J. Goura, V. Chandrasekhar, *Chem. Rev.* **2015**, *115*, 6854-6965.

[6] a) I. Lukes, J. Kotek, P. Vojtısek, P. Hermann, *Coord. Chem. Rev.* **2001**, *216-217*, 287-312. b) K. Nchimi Nono, A. Lecointre, M. Regueiro-Figueroa, C. Platas-Iglesias, L.C. Charbonnière L.J. *Inorg. Chem.* **2011**, *50*, 1689-1697. c) S. Abada, A. Lecointre, M. Elhabiri, D. Esteban-Gomez, C. Platas-Iglesias, G. Tallec, M. Mazzanti, L.J. Charbonnière, *Chem. Commun.* **2012**, *48*, 4085-4087.

[7] a) F.K. Kalman, M. Woods, P. Caravan, P. Jurek, M. Spiller, G. Tircso, R. Kiraly, E. Brücher, A.D. Sherry, *Inorg. Chem.* **2007**, *46*, 5260-5270. b) M. Botta, *Eur. J. Inorg. Chem.* **2000**, 399- 407. c) M. Elhabiri, A. Abada, M. Sy, A. Nonat, P. Choquet, D. Esteban-Gomez, C. Cassino, C. Platas-iglesias, M. Botta, L.J. Charbonnière, *Chem., Eur. J.*, **2015**, *21*, 6535-6546.

[8] a) D. Zeng, M. Ren, S.-S. Bao, L. Li, L.-M. Zheng, *Chem. Commun.* **2014**, *50*, 8356-8359. b) Y.-S. Ma, H. Li, J.-J. Wang, S.-S. Bao, R. Cao, Y.-Z. Li, J. Ma, L.-M. Zheng, *Chem. Eur. J.* **2007**, *13*, 4759-4769. c) Y.-S. Ma, Y. Song, L.-M. Zheng, *Inorg. Chim. Acta*, **2008**, *361*, 1363-1371. d) R.C. Holz, G.E. Meister, W. Dew. Horrocks, Jr *Inorg. Chem.* **1990**, *29*, 5183-5189. b) S.T. Frey, W. Dew. Horrocks, Jr *Inorg. Chem.* **1991**, *30*, 1073-1079. e) J. Salaam, L. Tabti, S. Bahamyirou, A. Lecointre, O. Hernandez Alba, O. Jeannin, F. Camerel, S. Cianférani, E. Bentouhami, A.M. Nonat, L.J. Charbonnière, *Inorg. Chem.* **2018**, *57*, 6095-6106. f) N. Souri, P. Tian, A. Lecointre, Z. Lemaire, S. Chafaa, J.M. Strub, S. Cianférani-Sanglier, M. Elhabiri, C. Platas-Iglesias, L.C. Charbonnière *Inorg. Chem.* **2016**, *55*, 12962-12974.

[9] a) N. Souri, P. Tian, C. Platas-Iglesias, S. Chafaa, K.L. Wong, A. Nonat, L.J. Charbonnière, *J. Am. Chem. Soc.* **2017**, 139, 1456-1459. b) A. Nonat, S. Bahamyrou, A. Lecointre, F. Przybilla, Y. Mély, C. Platas-Iglesias, F. Camerel, O. Jeannin, L.J. Charbonnière, *J. Am. Chem. Soc*. **2019,** *141*, 1568-1576.

[10] C. Charpentier, J. Salaam, A. Lecointre, O. Jeannin, A. Nonat, L.J. Charbonnière; *Eur. J. Inorg. Chem.* **2019**, 2168-2174.

[11] a) A. Nonat, C. Gateau, P. Fries, M. Mazzanti, *Chem. Eur. J.* **2006**, *12*, 7133-7150. b) F.K. Kalman, A. Vegh, M. Regueiro-Figueroa, E. Toth, C. Platas-Iglesias, G. Tircso, *Inorg. Chem.* **2015**, *54*, 2345-2356.

[12] a) C.F.G.C. Geraldes, A.D. Sherry, W.P. Cacheris, *Inorg. Chem.* **1989**, *28*, 3336-3341. b) J. Brandel, A. Lecointre, J. Kollek, S. Michel, V. Hubscher-Bruder, I. Déchamps-Olivier, C. Platas-Iglesias, L.C. Charbonnière, *Dalton Trans.* **2014**, *43*, 9070-9080.

[13] a) J. Kotek, P. Bebduskova, P. Hermann, L. Vander Elst, R.N. Muller, C.F.G.C. Geraldes, T. Maschmeyer, I. Lukes, J.A. Peters, *Chem. Eur.*

J. **2003**, *9*, 5899-5915. b) M. Mato-Iglesias, E. Balogh, C. Platas-Iglesias, E. Toth, A. de Blas, T. Rodriguez-Blas, *Dalton Trans.* **2006**, 5404-5415.

[14] Y. Bretonnière, M. Mazzanti, J. Pécaut, F.A. Dunand, A.E. Merbach, *Chem. Commun.* **2001**, 621-622.

[15] G. Anderegg, *Pure Appl. Chem.* **1982**, *54*, 2693-2758.

[16] W.R. Harris, K.N. Raymond, F.L. Weitl, *J. Am. Chem. Soc.* **1981**, *103*, 2667- 2675.

[17] a) C.J. Jocher, M. Botta, S. Avedano, E.G. Moore, J. Xu, S. Aime, K.N. Raymond, *Inorg. Chem.* **2007**, *46*, 4796-4798. b) M.K. Thompson, M. Botta, G. Nicolle, L. Helm, S. Aime, A.E. Merbach, K.N. Raymond, *J. Am. Chem. Soc.* **2003**, *125*, 14274-14275.

[18] C. Paul-Roth, K.N. Raymond, *Inorg. Chem.* **1995**, *34*, 1408-1412.

[19] a) E. Ventola, K. Rissanen, P. Vainiotalo, *Chem. Commun.* **2002**, 1110-1111. b) J. Ding, R.J. Anderegg, *J. Am. Soc. Mass Spectrom.* **1995**, *6*, 159-164.

[20] a) R. Janicki, A. Kedziorski, A. Mondry, Phys. Chem. Chem. Phys. **2016**, *18*, 27808-27817. b) F. Avecilla, J.A. Peters, C.F.G.C. Geraldes, *Eur. J. Inorg. Chem.* **2003**, 4179.

[21] R.D. Shannon *Acta Cryst.* **1976**, *A32*, 751-767.

[22] Assuming ionic radii of 1.120 Å and 1.095 Å respectively for Eu and Tb with a CN = 9 (reference 21), the corrected $d_{Ln\text{-}Ntert}$ becomes 2.699 Å for Tb compared to 2.693 Å for Eu.

[23] N. Vologdin, G.A. Rolla, M. Botta, L. Tei, *Org. Biomol. Chem.*, **2013**, *11*, 1683-1690.

[24] M. P. Lowe, D. Parker, O. Reany, S. Aime, M. Botta, G. Castellano, E. Gianolio, R. Pagliarin, *J. Am. Chem. Soc.* **2001**, *123*, 7601–7609.

[25] S. Aime, M. Botta, D. Esteban-Gomez, C. Platas-Iglesias, *Mol. Phys.* **2019**, *117*, 898-909.

[26] a) L. Banci, I. Bertini, C. Luchinat, C. Nuclear and Electron Relaxation. The Magnetic Nucleus-Unpaired Electron Coupling in Solution; VCH:Weinheim, Germany, **1991**; b) N. Bloembergen, L.O. Morgan, *J. Chem. Phys.* **1961**, *34*, 842−850.

[27] J.H. Freed, *J. Chem. Phys.* **1978**, *68*, 4034–4037.

[28] L. Tei, M. Botta, C. Lovazzano, A. Barge, L. Milone, S. Aime, *Magn. Reson. Chem.* **2008**, *46*, S86–S93.

[29] J. Rudovský, P. Cígler, J. Kotek, P. Hermann, P. Vojtíšek, I. Lukeš, J.A. Peters, L. Vander Elst, R.N. Muller R. N. *Chem. Eur. J.* **2005**, *11*, 2373‑2384.

[30] a) M. Mato-Iglesias, C. Platas-Iglesias, K. Djanashvili, J.A. Peters, E. Toth, E. Balogh, R.N. Muller, L. Vander Elst, A. de Blas, T. Rodriguez-Blas, *Chem. Commun.* **2005**, 4729-4731. b) E. Balogh, M. Mato-Iglesias, C. Platas-Iglesias, E. Toth, K. Djanashvili, J.A. Peters, A.; de Blas, T. Rodriguez-Blas, *Inorg. Chem.* **2006**, *45*, 8719-8728.

[31] A. Rodríguez-Rodríguez, D. Esteban-Gómez, A. de Blas, T. Rodríguez-Blas, M. Fekete, M. Botta, R. Tripier, C. Platas-Iglesias, *Inorg. Chem.* **2012**, *51*, 2509−2521.

[32] H.D. Powell, O.M. Ni Dhubhghaill, D. Pubanz, L. Helm, Y. Lebedev, W. Schlaepfer, A.E. Merbach, *J. Am. Chem. Soc.* **1996**, *118*, 9333-9346.

[33] a) W.d.W. Horrocks, D.R. Sudnick, *Acc. Chem. Res.* **1981**, *14*, 384-392. b) R.D. Supkowski, W.d.W. Horrocks, *Inorg. Chim. Acta.* **2002**, *340*, 44-48.

[34] A. Beeby, I.M. Clarkson, R.S. Dickins, S. Faulkner, D. Parker, L. Royle, A.S. de Sousa, J.A.G. Williams, M. Woods, *J. Chem. Soc., Perkin Trans. 2* **1999**, 493-503.

[35] K. Mikkelsen, S.O. Nielsen, *J. Phys. Chem.* **1960**, *64*, 632-637.

[36] A. Roca-Sabio, C. Bonnet, M. Mato-Iglesias, D. Esteban-Gomez, E. Toth, A. de Blas, T. Rodriguez-Blas, C. Platas-Iglesias, *Inorg. Chem.* **2012**, *51*, 10893-10903.

[37] a) A. Wacker, F. Carniato, C. Platas-Iglesias, D. Esteban-Gomez, H.J. Wester, L. Tei, J. Notni, *Dalton Trans.* **2017**, *46*, 16828-16836. b) A. Rodriguez-Rodriguez, Z. Garda, E. Ruscsak, D. Esteban-Gomez, A. de Blas, T. Rodriguez-Blas, L. Lima, M. Beyler, R. Tripier, G. Tircso, C. Platas-Iglesias, *Dalton Trans.* **2015**, *44*, 5017-5031.

[38] a) J.A. Peters, J. Huskens, D.J.; Raber, *Prog. Nucl. Magn. Reson. Spectrosc.* **1996**, *28*, 283-350; b) J.H. Forsberg, R. Delaney, Q. Zhao, G. Harakas, R. Chandran, *Inorg. Chem.* **1995**, *34*, 3705-3715. c) I. Bertini, C. Luchinat, G. Parigi, *Prog. Nucl. Magn. Reson. Spectrosc.* **2002**, *40*, 249-273.

[39] D. Esteban-Gomez, L.A. Büldt, P. Perez-Lourido, L. Valencia, M. Seitz, C. Platas-Iglesias, *Inorg. Chem.* **2019**, *58*, 3732-3743.

[40] a) K. Mason, A.C. Harnden, C.W. Patrick, A.W.J. Poh, A.S. Batnasov, E.A. Suturina, M. Vonci, E.J.L. Mc Innes, N.F. Chilton, D. Parker, *Chem. Commun.* **2018**, *54*, 8486-8489; b) M. Vonci, K. Mason, E.A. Suturina, A.T. Frawley, S.G. Worswick, I. Kuprov, D. Parker, E.J.L. Mc Innes, N.F. Chilton, *J. Am. Chem. Soc.* **2017**, *139*, 14166-14172. c) E.A. Suturina, K. Mason, C.F.G.C. Geraldes, I. Kuprov, D. Parker, *Angew. Chem. Int. Ed.* **2017**, *56*, 12215-12218.

[41] See for example a) O.A. Blackburn, N.F. Chilton, K. Keller, C.E. Tait, W.K. Myers, E.J.L. Mc Innes, A.M. Kenwright, P.D. Beer, C.R. Timmel, S. Faulkner, *Angew. Chem. Int. Ed.* **2015**, *54*, 10783-10786. b) T. Liu, A. Nonat, M. Beyler, M. Regueiro-Figueroa, K. Nchimi Nono, O. Jeannin, F. Camerel, F. Debaene, S. Cianférani-Sanglier, R. Tripier, C. Platas-Iglesias, L.J. Charbonnière, *Angew. Chem. Int. Ed.* **2014**, *53*, 7259-7263.

[42] D. Esteban-Gómez, A. de Blas, T. Rodríguez-Blas, L. Helm, C. Platas-Iglesias, *Chem. Phys. Chem.* **2012**, *13*, 3640-3650.

[43] M. Regueiro-Figueroa, C. Platas-Iglesias, *J. Phys. Chem. A* **2015**, *119*, 6436-6445.

[44] a) E.J. Corey, J.C. Bailar, *J. Am. Chem. Soc*. **1959**, *81*, 2620-2629; b) J.K. Beattie, *Acc. Chem. Res*. **1971**, *4*, 253-259.

[45] L. Helm, J.R. Morrow, C.J. Bond, F. Carniato, M. Botta, M. Braun, Z. Baranyai, R. Pujales-Paradela, M. Regueiro-Figueroa, D. Esteban-Gómez, C. Platas-Iglesias, T.J. Scholl, T. J. Contrast Agents for MRI: Experimental Methods. V.C. Pierre, M.J. Allen, Eds., The Royal Society of Chemistry, Croydon, UK, ch. 2.

[46] a) S. Khan, A. Kubica-Misztal, D. Kruk, J. Kowalewski, M. Odelius, *J. Chem. Phys.* **2015**, *142*, 034304. b) S. Khan, R. Pollet, R. Vuilleumier, J. Kowalewski, M. Odelius, *J. Chem. Phys.* **2017**, *147*, 244306; c) A. Lasoroski, R. Vuilleumier, R. Pollet, *J. Chem. Phys.* **2014**, *141*, 014201; d) C. Platas-Iglesias, D. Esteban-Gómez, L. Helm, M. Regueiro-Figueroa, *J. Phys. Chem. A* **2016**, *120*, 6467-6476.

[47] a) S. Rast, A. Borel, L. Helm, E. Belorizky, P.H. Fries, A.E. Merbach, *J. Am. Chem. Soc.* **2001**, *123*, 2637-2644; b) P.H. Fries, E. Belorizky, *ChemPhysChem* **2012**, *13*, 2074-2081.

[48] M.P. Lowe, D. Parker, O. Reany, S. Aime, M. Botta, G. Castellano, E. Gianolio, R. Pagliarin, *J. Am. Chem. Soc.* **2001**, *123*, 7601-7609.

[49] a) S. Aime, E. Gianolio, E. Terreno, G.B. Giovenzana, R. Pagliarin, M. Sisti, G. Palmisano, M. Botta, M.P. Lowe, D. Parker, *JBIC* **2000**, *5*, 488-497. b) P. Caravan, N.J. Cloutier, M.T. Greenfield, S.A. McDermid, S.U. Dunham, J.W.M. Bulte, J.C. Amedio, R.J. Looby, R.M. Supkowski, W.d.W. Horrocks, T.J. McMurry, R.B. Lauffer, R.B. *J. Am. Chem. Soc.* **2002**, *124*, 3152-3162.

[50] a) J.I. Bruce, R.S. Dickins, L.J. Govenlock, T. Gunnlaugsson, S. Lopinski, M.P. Lowe, D. Parker, R.D. Peacock, J.J.B. Perry, S. Aime, M. Botta, *J. Am. Chem. Soc.* **2000**, *122*, 9674-9684. b) V. Kubíček, A. Hamplová, L. Maribé, S. Mameri, R. Ziessel, E. Tóth, L.J. Charbonnière, *Dalton Trans* **2009**, 9466-9474.

Entry for the Table of Contents (Please choose one layout)

Layout 1:

RESEARCH ARTICLE

Text for Table of Contents: Around physiological pH, a pH dependent hydration change is observed in a Gd complex engendering large changes in its relaxivity properties. Protonation of the ligand induces hydrogen bonding within the phosphonated arms with the concomitant entry of a second water molecule.

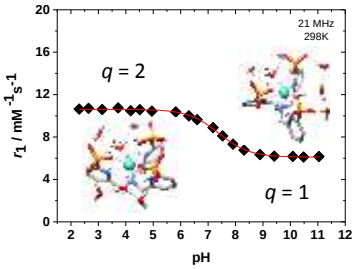

*Author(s), Corresponding Author(s)**

Page No. – Page No.

Title